



1 **Contrasting sources and processes of particulate species in haze days with low and**
2 **high relative humidity in wintertime Beijing**

3 Ru-Jin Huang¹, Yao He¹, Jing Duan¹, Yongjie Li², Qi Chen³, Yan Zheng³, Yang Chen⁴, Weiwei
4 Hu⁵, Chunshui Lin¹, Haiyan Ni¹, Wenting Dai¹, Junji Cao¹, Yunfei Wu⁶, Renjian Zhang⁶, Wei
5 Xu^{1,7}, Jurgita Ovadnevaite⁷, Darius Ceburnis⁷, Thorsten Hoffmann⁸, Colin D. O'Dowd⁷

6 ¹State Key Laboratory of Loess and Quaternary Geology, Center for Excellence in
7 Quaternary Science and Global Change, and Key Laboratory of Aerosol Chemistry and
8 Physics, Institute of Earth and Environment, Chinese Academy of Sciences, Xi'an 710061,
9 China

10 ²Department of Civil and Environmental Engineering, Faculty of Science and Technology,
11 University of Macau, Taipa, Macau, China

12 ³State Key Joint Laboratory of Environmental Simulation and Pollution Control, College
13 of Environmental Sciences and Engineering, Peking University, Beijing 100871, China

14 ⁴Chongqing Institute of Green and Intelligent Technology, Chinese Academy of Sciences,
15 Chongqing 400714, China

16 ⁵State Key Laboratory of Organic Geochemistry and Guangdong Key Laboratory of
17 Environmental Protection and Resources Utilization, Guangzhou Institute of
18 Geochemistry, Chinese Academy of Sciences, Guangzhou 510640, China

19 ⁶RCE-TEA, Institute of Atmospheric Physics, Chinese Academy of Sciences, Beijing
20 100029, China

21 ⁷School of Physics and Centre for Climate and Air Pollution Studies, Ryan Institute,
22 National University of Ireland Galway, University Road, Galway H91CF50, Ireland

23 ⁸Institute of Inorganic and Analytical Chemistry, Johannes Gutenberg University of
24 Mainz, Duesbergweg 10-14, 55128 Mainz, Germany

25 *Correspondence to:* Ru-Jin Huang (rujin.huang@ieecas.cn)

26

27 **Abstract**

28 Although there are many studies of particulate matter (PM) pollution in Beijing, the
29 sources and processes of secondary PM species during haze periods remain unclear.
30 Limited studies have investigated the PM formation in highly-polluted environments
31 under low and high relative humidity (RH) conditions. Herein, we present a systematic
32 comparison of species in submicron particles (PM₁) in wintertime Beijing (29 December
33 2014 to 28 February 2015) for clean periods and pollution periods under low and high
34 RH conditions. PM₁ species were measured with an aerosol chemical species monitor
35 (ACSM) and an aethalometer. Sources and processes for organic aerosol (OA) were
36 resolved by positive matrix factorization (PMF) with multilinear engine 2 (ME-2). The
37 comparisons for clean, low-RH pollution, and high-RH pollution periods are made from
38 three different aspects, namely (a) mass concentration, (b) mass fraction, and (c) growth
39 rate in diurnal profiles. OA is the dominant component of PM₁ with an average mass
40 concentration of 56.7 $\mu\text{g m}^{-3}$ (46%) during high-RH pollution and 67.7 $\mu\text{g m}^{-3}$ (54%)
41 during low-RH pollution periods. Sulfate had higher concentration and mass fraction



42 during high-RH pollution periods, while nitrate had higher concentration and mass
43 fraction during low-RH pollution periods. The diurnal variations of nitrate and
44 oxygenated organic aerosol (OOA) showed a daytime increase of their concentrations
45 during all three types of periods. Nitrate had similar growth rates during low-RH ($0.40 \mu\text{g}$
46 $\text{m}^{-3} \text{h}^{-1}$) and high-RH ($0.55 \mu\text{g} \text{m}^{-3} \text{h}^{-1}$) pollution periods. OOA had a higher growth rate
47 during low-RH pollution periods ($1.0 \mu\text{g} \text{m}^{-3} \text{h}^{-1}$) than during high-RH pollution periods
48 ($0.40 \mu\text{g} \text{m}^{-3} \text{h}^{-1}$). In contrast, sulfate had a decreasing trend during low-RH pollution
49 periods, while it increased significantly with a growth rate of $0.81 \mu\text{g} \text{m}^{-3} \text{h}^{-1}$ during high-
50 RH pollution periods. These distinctions in mass concentrations, mass fractions, and
51 daytime growth rates may be explained by the difference in the formation processes,
52 affected by meteorological conditions. In particular, photochemical oxidation and
53 aqueous-phase processes may both produce sulfate and nitrate. The relative importance
54 of the two pathways, however, differs under different meteorological conditions.
55 Additional OOA formation under high-RH (>70%) conditions suggests aqueous-related
56 formation pathways. This study provides a general picture of the haze formation in Beijing
57 under different meteorological conditions.

58 **1 Introduction**

59 Air pollution is a serious environmental problem in China, particularly in the North China
60 Plain (NCP) in winter, affecting air quality and human health. Beijing is one of the most
61 polluted megacities in the NCP, with an annual mean concentration of $\text{PM}_{2.5}$ being 86 and
62 $51 \mu\text{g} \text{m}^{-3}$ in 2014 and 2018, respectively (<http://sthjj.beijing.gov.cn/>), which significantly
63 exceeded the Chinese National Ambient Air Quality Standard (annual average of $35 \mu\text{g} \text{m}^{-3}$).
64 Fine PM pollution in polluted urban environments is complex and is typically
65 associated with enhanced primary emissions from multiple sources, strong secondary
66 aerosol formation, and stagnant weather conditions (Sun et al., 2011; 2013; 2016; Huang
67 et al., 2014; Hu et al., 2016; An et al., 2019). Regional transport of air pollutants from
68 urbanized and industrialized areas has an important contribution to fine PM pollution in
69 the NCP region. For example, severe fine PM pollution in Beijing during winter often
70 happened when prevailing air masses were from the south (Sun et al., 2016).

71 Organic aerosol (OA) is the major constituent of fine PM and is much less understood
72 compared to inorganic aerosol in terms of their chemical nature and sources (Hallquist et
73 al., 2009; Shrivastava et al., 2017). OA is composed of a wide variety of organic species
74 from different sources, and its emission sources and atmospheric processes are not well
75 understood so far, especially in those regions with high fine PM pollution. OA is either
76 directly emitted to the atmosphere (primary organic aerosol, POA) or formed in the
77 atmosphere (secondary organic aerosol, SOA). Therefore, it is essential to identify and
78 quantify the major emission sources and understand the formation processes of OA.

79 The Aerodyne aerosol chemical speciation monitor (ACSM) with quadrupole (Q) or time-
80 of-flight (TOF) mass analyzer is capable of real-time determination of non-refractory
81 components in submicron aerosol (NR-PM_1), overcoming the limitation of filter



82 measurements such as limited time resolution or measurement artifacts (Ng et al., 2011a;
83 Froehlich et al., 2013). ACSM has been widely used for fine PM studies in many sites in
84 China including Beijing, Nanjing, Shijiazhuang, and Baoji (Sun et al., 2014; Wang et al.,
85 2017; Zhang et al., 2017; Huang et al., 2019). By applying positive matrix factorization
86 (PMF, Paatero et al., 1993) or multilinear engine (ME-2, Canonaco et al., 2013) solver to
87 the ACSM data, main OA sources can be identified. Those sources include hydrocarbon-
88 like OA (HOA), biomass burning OA (BBOA), cooking OA (COA), coal combustion OA (CCOA)
89 and oxygenated OA (OOA). OOA can further be resolved into semi-volatile OOA (SV-OOA)
90 and low-volatility OOA (LV-OOA) by volatility, or more-oxidized OOA (MO-OOA) and less-
91 oxidized OOA (LO-OOA) by oxidation state. MO-OOA and LO-OOA together were found to
92 contribute 61% of OA in Beijing during summer in 2011 (Sun et al., 2012), while POA was
93 found to be more important during winter of the same year (Sun et al., 2013). However,
94 many recent studies show large contributions of SOA in wintertime Beijing (Huang et al.,
95 2014; Hu et al., 2016; Xu et al., 2018) and CCOA is often found to be a large fraction of POA
96 during wintertime pollution days in Beijing (Sun et al., 2016b; Wang et al., 2015; Elser et
97 al., 2016). The discrepancies in SOA contribution in different measurement periods reflect
98 the difference in atmospheric and meteorological conditions, e.g., atmospheric oxidative
99 capacity and relative humidity (RH) (Sun et al., 2013; Xu et al., 2017; Wu et al., 2018; Song
100 et al., 2019).

101 In this study, we present measurement results at an urban site in Beijing during the winter
102 of 2014–2015. The chemical nature of NR-PM₁, sources of OA, formation processing of
103 secondary aerosol in different episodes, and particularly the effects of RH on secondary
104 aerosol formation are discussed.

105 **2 Methods**

106 **2.1 Site description and instrumentation**

107 The online measurements were conducted on the rooftop of a building (about 20 m above
108 the ground level) at the campus of the National Centre for Nanoscience and Technology
109 (40.00° N, 116.38° E) from 29 December 2014 to 28 February 2015. The observation site
110 is between the 4th and 5th ring roads in the northwest of Beijing and is surrounded by a
111 residential area.

112 A Q-ACSM was deployed for the mass concentration measurements of NR-PM₁ species,
113 and the detailed operation principles can be found in Ng et al. (2011a). Briefly, ambient
114 air was pumped through a 3/8 in stainless steel tube at a flow rate of 3 L min⁻¹, of which
115 85 mL min⁻¹ was sampled into the Q-ACSM. In order to remove coarse particles, an URG
116 cyclone (URG-2000-30ED, size cut-off 2.5 μm) was installed in front of the inlet. Because
117 particle bounce can affect collection efficiency (CE), to reduce this uncertainty and to dry
118 the particles, a Nafion dryer (MD-110-48S; Perma Pure, Inc., Lakewood, NJ, USA) was
119 installed after the URG cyclone. An aerodynamic lens was used to focus the submicron
120 particles into a narrow beam, the particles beam then impinged on a heated tungsten



121 surface (about 600 °C) to evaporate, impacted by 70-eV electron to ionize, and then
122 detected by a quadrupole mass spectrometer. During this study, the scan rate of Q-ACSM
123 was at 200 ms amu⁻¹ from m/z 10 to 150 and the time resolution was 30 min. To determine
124 the response factor (RF), a differential mobility analyzer (DMA, TSI model 3080) and a
125 condensation particle counter (CPC, TSI model 3772) were used to select and count the
126 monodisperse 350-nm ammonium nitrate (NH₄NO₃) particles, respectively. The mass of
127 NH₄NO₃ particles was calculated with known particle size and number concentrations.
128 This calculated mass concentration was compared to the RF of the Q-ACSM, resulting in
129 the ionization efficiency (IE) value (Ng et al., 2011a).

130 The gaseous species including O₃ and NO_x were measured by a Thermo Scientific Model
131 49i ozone analyzer and a Thermo Scientific Model 42i NO–NO₂–NO_x analyzer, respectively.
132 The NH₃ concentrations were measured by an NH₃ analyzer (Picarro G2103). The
133 concentrations of black carbon (BC) was determined by an aethalometer (Model AE-33,
134 Magee Scientific) with a time resolution of 1 min. In brief, light attenuation at seven
135 different wavelengths was recorded for particle-laden filter spots, and BC concentration
136 was retrieved based on the light attenuation at 880 nm. An automatic weather station
137 (MAWS201, Vaisala, Vantaa, Finland) was used to measure the meteorological parameters
138 including temperature, pressure, relative humidity and visibility, and a wind sensor
139 (Vaisala Model QMW101-M2) was used to measure the wind speed and wind direction.

140 2.2 Data analysis

141 2.2.1 ACSM data analysis

142 The standard Q-ACSM data analysis software (v.1.5.3.5) written in Igor Pro (WaveMetrics,
143 Inc., OR, USA) was used to calculate the mass concentrations for different species in NR-
144 PM₁. Default relative ionization efficiencies (RIE) were used for organics (1.4), nitrate (1.1)
145 and chloride (1.4), respectively (Ng et al., 2011a). RIE of 5.8 for ammonium and 1.2 for
146 sulfate were determined by the IE calibrations of ammonium nitrate and ammonium
147 sulfate. Meanwhile, data were corrected for the particle collection efficiency (CE), due to
148 particle bounce on the vaporizer. CE can be affected by relative humidity, mass fraction of
149 ammonium nitrate and particle acidity. In our measurement, the particles were generally
150 neutral and dried before sampling into the ACSM. CE was calculated as $CE_{dry} = \max(0.45,$
151 $0.0833 + 0.9167 \times ANMF)$, where ANMF refers to the ammonium nitrate fraction in NR-
152 PM₁ (Middlebrook et al. 2012).

153 2.2.2 OA source apportionment

154 The receptor model PMF using a multilinear engine (ME-2) was used to identify and
155 quantify the OA sources. PMF is a bilinear receptor model used to describe the variability
156 of a multivariate dataset, X, as the linear combination of a set of constant factor profiles, F,
157 and their corresponding time series G, as expressed in equation 1.



158 $X = GF + E$ (1)

159 where X is the measured OA mass spectra consisting of i rows and j columns, and E is the
160 model residuals. The PMF uses a least squares method to minimize the object function Q ,
161 defined as the sum of the squared residuals (e_{ij}) weighted by their respective uncertainties
162 (σ_{ij}).

163 $Q = \sum_{i=1}^m \sum_{j=1}^n (e_{ij}/\sigma_{ij})^2$ (2)

164 Unconstrained PMF analyses of OA data suffer from rotational ambiguity when sources
165 show similar profiles and temporal covariation (Canonaco et al., 2013; Huang et al., 2019).
166 However, by introducing *a priori* information as additional model input and constraining
167 one or more output factor profiles to a predetermined range, ME-2 can overcome such
168 difficulties and provide more environmentally meaningful solutions. When an element of
169 a factor profile (f_j , where j refers to the m/z) is constrained with a certain a value (a), the
170 following conditions need to be fulfilled:

171 $f_{j,solution} = f_j \pm a \times f_j$ (3)

172 The a value can vary between 0 and 1, which is the extent to which the output profiles can
173 vary from the model inputs. The data analysis were conducted using the source finder
174 (SoFi, Canonaco et al., 2013) tool version 4.9 for Igor Pro. Due to rotational ambiguity,
175 there was no mathematically unique solution. Therefore, criteria including chemical
176 fingerprint of the factor profiles, correlations with external tracers, and diurnal cycles
177 were used for the factor identification and interpretation (Ulbrich et al., 2009; Huang et
178 al., 2014, Elser et al., 2016).

179 2.2.3 Aerosol liquid water content

180 NR-PM₁ inorganic species, NH₃ concentrations and meteorological parameters including
181 temperature and RH were used to calculate the aerosol liquid water content (ALWC)
182 based on the ISORROPIA-II model (Fountoukis and Nenes, 2007). Here we ran the
183 ISORROPIA-II in “forward” mode and the particles were assumed to be deliquescent, i.e.,
184 in metastable mode (Hennigan et al., 2015). The thermodynamic equilibrium of the NH₄⁺-
185 SO₄²⁻-NO₃⁻-Cl⁻-H₂O system was then modeled and ALWC was calculated.

186 3 Results and discussion

187 3.1 Temporal variations and mass fractions of PM₁ species

188 Fig. 1 shows the time series of mass concentrations of OA, SO₄²⁻, NO₃⁻, NH₄⁺, Cl⁻, and BC, as
189 well as the meteorological parameters. The average mass concentration of PM₁ during the
190 entire measurement period was 73.8 μg m⁻³, similar to those observed in Beijing in winter
191 2011 (66.8 μg m⁻³, Sun et al., 2013) and winter 2013 (64 μg m⁻³, Sun et al., 2016). The



192 lowest daily average concentration was $5.2 \mu\text{g m}^{-3}$ on 31 December, while the highest was
193 $210.1 \mu\text{g m}^{-3}$ on 15 January, with a difference of a factor of ~ 40 . OA (52%) was the most
194 abundant component of PM_{10} , irrespective of the meteorological conditions, followed by
195 nitrate (14%) and sulfate (11%). The weather conditions during the measurement period
196 were characterized by drastic changes in wind speed, wind direction, RH and temperature,
197 providing a unique setting to investigate the influence of meteorological conditions on PM
198 species. As such, the entire measurement period can be divided into the clean period (PM_{10}
199 $< 20 \mu\text{g m}^{-3}$) and the pollution period ($\text{PM}_{10} > 100 \mu\text{g m}^{-3}$). South/southeasterly wind
200 directions with low speed (average, $0.9 - 1.0 \text{ m s}^{-1}$) were typical for the pollution period,
201 while north/northwesterly with high speed (average, 2.5 m s^{-1}) for the clean period (Table
202 1).

203 To investigate the effects of RH on PM pollution formation, we further divided the
204 pollution period into two categories, the low-RH pollution days (RH $< 50\%$) and the high-
205 RH pollution days (RH $> 50\%$). The diurnal variations of mass concentrations and fractions
206 of different chemical species during clean days, low-RH pollution days and high-RH
207 pollution days are shown in Fig. 2. The mass fractional variations were flatter during low-
208 RH and high-RH pollution days than during clean days, likely due to the accumulation of
209 pollutants during stagnant weather conditions in pollution days. During clean days,
210 secondary inorganic aerosol showed generally increasing trends from 06:00 to 20:00 local
211 time (LT), despite the development of the boundary layer height during the day. The
212 growth rate of nitrate mass ($0.21 \mu\text{g m}^{-3} \text{ h}^{-1}$) was higher than that of sulfate ($0.04 \mu\text{g m}^{-3} \text{ h}^{-1}$)
213 and ammonium ($0.10 \mu\text{g m}^{-3} \text{ h}^{-1}$), indicating that formation of nitrate was perhaps faster
214 than that of sulfate and ammonium during clean days. During low-RH pollution days,
215 nitrate increased from 06:00 to 20:00 LT, with a growth rate of $0.40 \mu\text{g m}^{-3} \text{ h}^{-1}$, which was
216 two times higher than that during clean days. On the contrary, sulfate concentrations
217 increased from 06:00 to 10:00 LT, then started decreasing and reached the minimum at
218 14:00 LT, possibly due to the increase of the boundary layer height during the day, which
219 outweighed the production of sulfate. Associated with both sulfate and nitrate,
220 ammonium showed a minor increase from 06:00 to 20:00 LT with a mass growth rate of
221 $0.18 \mu\text{g m}^{-3} \text{ h}^{-1}$. This phenomenon suggested that the low-RH condition was favorable for
222 nitrate formation but not for sulfate formation under polluted conditions. In contrast,
223 obvious increases of secondary inorganic species from 8:00 to 16:00 LT were observed
224 during high-RH pollution days, with growth rates of $0.81 \mu\text{g m}^{-3} \text{ h}^{-1}$, $0.55 \mu\text{g m}^{-3} \text{ h}^{-1}$ and 0.46
225 $\mu\text{g m}^{-3} \text{ h}^{-1}$ for sulfate, nitrate and ammonium, respectively. These mass growth rates
226 increased correspondingly by about 20, 2.6 and 4.6 times compared to those during clean
227 days. Note that nitrate growth rate in high-RH pollution days ($0.55 \mu\text{g m}^{-3} \text{ h}^{-1}$) was still
228 slightly higher than that in low-RH pollution days ($0.40 \mu\text{g m}^{-3} \text{ h}^{-1}$), indicating that nitrate
229 production is still efficient when RH is high, although not as much higher compared to
230 sulfate. Measurements of sulfate oxygen isotopes suggest that the largely enhanced
231 formation of sulfate is associated with efficient aqueous-phase reactions during high-RH
232 pollution days (Shao et al., 2019).

233 3.2 Sources and diurnal variations of OA



234 Source apportionment was performed on the OA data. Three to seven factors were
235 examined using an unconstrained PMF model, and the factors were qualitatively identified
236 based on their mass spectral profiles and correlation with external data. We found that a
237 solution of five factors (i.e., HOA, COA, CCOA, BBOA, and OOA) best explains our data. For
238 the solutions with less than 5 factors, HOA appeared to be mixed with COA while CCOA
239 mixed with BBOA (Fig. S1). However, when the number of factors was increased to 6, the
240 OOA factor split into two OOA factors of similar time series (Fig. S2), suggesting that
241 further separation of the factors does not improve the interpretation of the data.

242 Although five factors with different profiles and temporal variations were identified by
243 the unconstrained PMF model, the factor profiles and time series were suboptimal,
244 specifically for HOA, COA, and BBOA. The diurnal pattern of HOA showed pronounced
245 peaks at cooking time, indicating its mixing with COA. The fractional contribution of m/z
246 60 (f_{60} , typically related to the fragmentation of anhydrous sugars) in HOA (0.008) was
247 higher than the average value reported from multiple ambient datasets (0.002, Ng et al.,
248 2011). To reduce the mixing between factors, the reference HOA mass spectral profile,
249 characterized by a small f_{60} (Wang et al., 2017), and the BBOA mass spectral profile,
250 derived from Beijing wintertime measurements (Elser et al., 2016), were constrained
251 using ME-2. For the COA mass spectral profile that was derived from our unconstrained
252 PMF analysis, a-value of 0 was used. Meanwhile, for HOA and BBOA, the a values were
253 varied systematically between 0 and 1 with an interval of 0.1 to explore the solution space.
254 To assess the obtained solutions, we have set thresholds for the highest acceptable f_{60}
255 value (0.006) for HOA and f_{57} value (0.042) for BBOA, based on mass spectra obtained at
256 multiple sites (mean $\pm 2\sigma$, Ng et al., 2011). Only solutions that conform to both criteria
257 were selected and the final solution was the average of those selected reasonable
258 solutions (Fig. S3).

259 The final OA factors resolved by ME-2 include four POA (i.e., HOA, COA, BBOA and CCOA),
260 and one SOA (i.e., OOA) factors, on average accounting for 14%, 14%, 10%, 32% and 31%
261 of OA mass concentration, respectively. The mass spectral profiles and time series of the
262 resolved factors are shown in Fig. 3a and b, respectively. The diurnal patterns of these
263 factors are presented in Fig. 4. The HOA spectrum is similar to those derived from other
264 studies in Beijing (Hu et al., 2016; Sun et al., 2014; 2016) and Pittsburgh (Ulbrich et al.,
265 2016), and also resembles the source profile from diesel exhausts (Canagaratna et al.,
266 2004). A strong correlation between the time series of HOA and BC was observed
267 ($R^2=0.84$). The diurnal cycle of HOA was similar to those observed in other studies in
268 Beijing (Sun et al., 2011; 2013; 2014), showing higher mass concentrations during the
269 night than during the day, due to enhanced traffic emissions from heavy duty vehicles and
270 diesel trucks that are allowed to enter the inner city during the night.

271 Similar to HOA, the mass spectrum of COA also displayed high signals in odd fragments,
272 while the m/z 55/57 ratio (1.45) and m/z 41/43 ratio (1.6) were significantly higher
273 compared to those of the HOA factor profile (m/z 55/57=0.65, m/z 41/43=0.88). The COA
274 profile is similar to those resolved in previous studies in Beijing (Elser et al., 2016; Sun et



275 al., 2016), Paris (Crippa et al., 2013) and Zurich (Dey et al., 2004). The R^2 between COA
276 and m/z 55 time series was 0.73. The diurnal cycle of COA showed two prominent peaks
277 during lunch (12:00-13:00 LT) and dinner (18:00-19:00 LT) times, and the peak in the
278 evening was more pronounced than that at noon, consistent with a previous study in
279 Beijing (Sun et al., 2016). Furthermore, the diurnal variation of COA was more obvious
280 with much clear noon and evening peaks during clean days than during low-RH and high-
281 RH pollution days, likely because the stagnant meteorological conditions during pollution
282 days facilitated the accumulation of pollutants and thus weakened the diurnal fluctuation.

283 The BBOA mass spectrum showed a similar pattern as that extracted from Crippa et al.
284 (2014), with pronounced peaks at m/z 60 and 73, two distinct markers of biomass
285 burning emissions (Lanz et al., 2007). BBOA also showed similar time series with a high
286 signal at m/z 60 ($R^2=0.74$). The diurnal cycle of BBOA showed a slight increase during the
287 night (18:00-24:00 LT), corresponding to nighttime burning for residential heating in
288 clean days, while this diurnal cycle became much flat during low-RH and high-RH
289 pollution days, likely due to the stagnant meteorological conditions during pollution days.
290 On average, BBOA contributed 10% of the total OA, much less than that of CCOA (32%),
291 consistent with previous results in Beijing (Elser et al., 2016).

292 The profile of CCOA showed a moderate correlation with that resolved in Beijing in winter
293 2014 (Elser et al., 2016). Similar to previous studies, signals related to unsaturated
294 hydrocarbons, especially those at m/z 77, 91 and 115, contributed significantly to the total
295 CCOA signal. In addition, there was a strong correlation between CCOA and Cl^- ($R^2=0.82$),
296 which was considered as a marker mainly from coal combustion emissions. The mass
297 concentration and mass fraction of CCOA were both significantly higher at night than
298 those during the day, which was observed both in clean days and pollution days. The
299 diurnal pattern suggests much stronger emissions from coal combustion at night, a
300 situation further deteriorated by a shallower boundary layer at night.

301 One secondary OA factor, namely OOA, was also resolved, characterized by an important
302 contribution at m/z 44. The profile of OOA is also similar to those resolved in Ng et al.
303 (2011) and Sun et al. (2013). OOA is correlated well with nitrate ($R^2=0.89$). and the
304 diurnal cycle of OOA shows an increase from about 6:00 to 20:00 LT, indicating the
305 contribution from photochemical production. Note that the growth rate of OOA during
306 low-RH pollution days ($1.0 \mu\text{g m}^{-3} \text{h}^{-1}$) was higher than that during high-RH pollution days
307 ($0.40 \mu\text{g m}^{-3} \text{h}^{-1}$) and clean days ($0.35 \mu\text{g m}^{-3} \text{h}^{-1}$) (Fig. 4).

308 3.3 Chemically resolved PM pollution

309 Fig. 5 shows the mass fraction of PM_{10} and OA during clean, low-RH and high-RH pollution
310 periods. OA was the dominant component in PM_{10} , with an average concentration
311 increasing from $10.9 \mu\text{g m}^{-3}$ during clean periods to $56.7 \mu\text{g m}^{-3}$ during high-RH pollution
312 periods and further to $67.7 \mu\text{g m}^{-3}$ during low-RH pollution periods. The corresponding
313 mass fraction of OA was 56%, 46%, and 54%, respectively. The decrease of OA mass



314 fraction during pollution periods can be attributed to the increased formation of sulfate
315 and nitrate, as demonstrated in the above section. Specifically, nitrate increased from 11%
316 ($2.2 \mu\text{g m}^{-3}$) during clean periods to 14% ($17.2 \mu\text{g m}^{-3}$) during high-RH pollution periods
317 and to 15% ($18.8 \mu\text{g m}^{-3}$) during low-RH pollution periods, while sulfate increased from
318 10% ($2.0 \mu\text{g m}^{-3}$) during clean periods to 17% ($20.9 \mu\text{g m}^{-3}$) during high-RH pollution
319 periods but decreased back to as low as 7% ($8.8 \mu\text{g m}^{-3}$) during low-RH pollution periods.
320 The increased formation of nitrate from clean to pollution periods, especially during low-
321 RH pollution periods, is likely due to enhanced photochemical production, as discussed in
322 Lu et al. (2019) which shows fast photochemistry during wintertime haze events in
323 Beijing. Specifically, the atmospheric oxidation proxy ($\text{O}_x = \text{O}_3 + \text{NO}_2$) increased from 39.2
324 ppb during clean periods to 47.8 ppb during high-RH pollution periods, and up to as high
325 as 59.8 ppb during low-RH pollution periods. Meanwhile, the precursor gas for nitrate,
326 NO_2 , increased accordingly from 16.7 ppb during clean periods to 64.3 ppb during high-
327 RH pollution periods and to 103.0 ppb during low-RH pollution periods. The averaged
328 PM_{10} concentrations during high-RH ($123.2 \mu\text{g m}^{-3}$) and low-RH ($125.4 \mu\text{g m}^{-3}$) pollution
329 periods were very similar, but a distinct difference lies in the sulfate and nitrate fractions
330 in these two types of pollution periods. We observed a much larger contribution from
331 nitrate during low-RH pollution periods than during high-RH pollution periods, which
332 may be due to enhanced photochemical formation and also contributions of N_2O_5 uptake,
333 and a much larger contribution from sulfate during high-RH pollution periods than during
334 low-RH pollution periods because of enhanced formation from aqueous-phase processes.

335 In terms of OA sources, CCOA and OOA were the major sources irrespective of the PM_{10}
336 level. The mass fraction of CCOA in OA increased from 25% ($2.8 \mu\text{g m}^{-3}$) during clean
337 periods to 31% ($17.6 \mu\text{g m}^{-3}$) during high-RH pollution periods and to 35% ($23.7 \mu\text{g m}^{-3}$)
338 during low-RH pollution periods, indicating the important contribution of residential coal
339 combustion emissions. OOA also increased significantly during pollution periods, from 4.1
340 $\mu\text{g m}^{-3}$ to $\sim 20 \mu\text{g m}^{-3}$. It should be noted that the average OOA mass concentrations were
341 rather similar during high-RH ($19.8 \mu\text{g m}^{-3}$) and low-RH ($18.3 \mu\text{g m}^{-3}$) pollution periods.
342 However, the OOA mass fraction in OA during the high-RH pollution period (35%) is
343 higher than that during the low-RH pollution period (27%), indicating an additional
344 contribution of OOA from e.g., aqueous-phase oxidations during high RH condition, as
345 discussed below. The mass fraction of HOA in OA increased from 8% ($0.8 \mu\text{g m}^{-3}$) during
346 clean days to 13% ($8.8 \mu\text{g m}^{-3}$) during low-RH pollution days and further to 16% ($9.1 \mu\text{g m}^{-3}$)
347 during high-RH pollution days, suggesting an increased contribution of HOA in
348 pollution days. The mass fraction of HOA is similar to those measured in wintertime
349 Beijing in 2011 (14%, Hu et al., 2016) and in 2013 (11%, Sun et al., 2016). In contrast, the
350 mass concentrations of COA during low-RH pollution days ($8.8 \mu\text{g m}^{-3}$) and high-RH
351 pollution days ($6.8 \mu\text{g m}^{-3}$) were higher than that during clean days ($2.0 \mu\text{g m}^{-3}$), but the
352 mass fraction of COA in OA during high-RH pollution days (12%) and low-RH pollution
353 days (13%) were lower than that during clean days (20%). A similar decrease of HOA
354 contribution and increase of COA contribution during clean days were also observed by
355 Sun et al. (2016) in wintertime Beijing in 2011. The highest contribution of BBOA was
356 observed during low-RH pollution days with a mass fraction of 12% ($8.1 \mu\text{g m}^{-3}$). The



357 BBOA concentration during high-RH pollution days ($3.4 \mu\text{g m}^{-3}$) was higher than that
358 during clean days ($1.0 \mu\text{g m}^{-3}$), but the mass fraction of BBOA in OA during high-RH
359 pollution days (6%) was lower than that during clean days (10%).

360 The chemical composition and sources of PM_{10} under different meteorological conditions
361 (e.g., wind direction, wind speed and RH) in the seven pollution episodes ($\text{PM}_{10} > 100 \mu\text{g m}^{-3}$)
362 and seven clean episodes ($\text{PM}_{10} < 20 \mu\text{g m}^{-3}$) are shown in Fig. S4. Note that these
363 episodes in total accounted for 91% of the entire measurement period. The pollution
364 episodes were found to be associated with the air masses from south/southwest, while
365 clean episodes were associated with the air masses from north/northwest. Meanwhile,
366 the pollution episodes were generally associated with higher RH and lower wind speeds
367 when compared to the clean episodes. The wind speeds were approximately three times
368 higher in clean episodes than those in pollution episodes. For example, the lowest
369 concentration of PM_{10} was $6.7 \mu\text{g m}^{-3}$ in C6 period, corresponding to the highest wind speed
370 (4 m s^{-1}) and the lowest concentrations ($< 20 \text{ ppb}$) of inorganic gaseous precursors (SO_2 ,
371 NH_3 , and NO_x), while the highest PM_{10} concentration of $169 \mu\text{g m}^{-3}$ was found at P5,
372 corresponding to a much lower wind speed ($< 1 \text{ m s}^{-1}$). The mass concentrations of OA
373 increased from $\sim 4.1\text{--}9.4 \mu\text{g m}^{-3}$ during clean episodes to $\sim 44.7\text{--}85.7 \mu\text{g m}^{-3}$ during
374 pollution episodes. However, the contributions of OA to PM_{10} showed a decreasing trend
375 from 48–59% during clean episodes to 44–57% during pollution episodes, and the
376 corresponding contributions of secondary inorganic species increased from 29–34%
377 ($\sim 2.2\text{--}5.5 \mu\text{g m}^{-3}$) to 27–47% ($\sim 25.5\text{--}62.1 \mu\text{g m}^{-3}$), indicating a notable production and
378 accumulation of secondary inorganic aerosol during haze pollution episodes. In contrast,
379 the mass concentration of OOA increased from $\sim 1.4\text{--}3.9 \mu\text{g m}^{-3}$ during clean episodes to
380 $\sim 10.0\text{--}27.6 \mu\text{g m}^{-3}$ during pollution episodes, while the contribution of OOA to OA
381 decreased from 33–64% during clean episodes to 20–52% during pollution episodes. The
382 corresponding contribution of POA sources increased from 35–67% ($\sim 1.2\text{--}4.7 \mu\text{g m}^{-3}$) to
383 38–80% ($\sim 13.9\text{--}58.7 \mu\text{g m}^{-3}$), suggesting that in general the emission and accumulation of
384 POA sources played an important role during haze pollution in this measurement
385 campaign.

386 Comparing the pollution episodes with different RH conditions (see Fig. S4), the mass
387 fraction of sulfate was much higher during high-RH pollution episodes (P3, P6 and P7, 15–
388 21%) than during low-RH pollution episodes (P1, P2, P4 and P5, 6–8%). OOA also showed
389 a much higher contribution to OA during high-RH pollution events (P6, P7, 50–62%) than
390 during low-RH pollution events (P1–P5, 20–31%). These variations suggest the potential
391 importance of aqueous-phase reactions on the formation of sulfate and OOA, as discussed
392 above. Further comparison of high-RH and low-RH pollution episodes with similar PM_{10}
393 levels (e.g., P2 and P6 with PM_{10} concentration of $98.8 \mu\text{g m}^{-3}$ and $99.6 \mu\text{g m}^{-3}$, respectively)
394 shows that secondary inorganic aerosol dominated PM_{10} at high-RH pollution episode.
395 Similarly, as for the high-RH and low-RH pollution episodes with similar OA levels, for
396 example, P6 ($44.7 \mu\text{g m}^{-3}$) and P7 ($46.3 \mu\text{g m}^{-3}$), OOA dominated the particulate pollution
397 (62% of OA) at high-RH pollution events due to efficient formation of SOA. On the contrary,
398 POA had increased contributions to PM_{10} pollution at low RH and stagnant weather



399 conditions (from 38% of OA at high-RH pollution to 50% of OA at low-RH pollution),
400 consistent with previous studies in other Chinese cities (e.g., Wang et al., 2017; Huang et
401 al., 2019). These results indicate that meteorological conditions have important effects on
402 the particulate pollution.

403 3.4 Formation of secondary aerosol

404 The relationship between SO_4^{2-} and NO_3^- is investigated to elucidate the formation
405 processes of these two typical secondary inorganic aerosol species. The correlation
406 between SO_4^{2-} and NO_3^- was weak for the entire pollution period, because of the varied
407 relative contribution of different formation processes during different periods. However,
408 better correlations between SO_4^{2-} and NO_3^- were found with different slopes when the data
409 were divided into low-RH (RH <50%) and high-RH (RH >50%) pollution periods (Fig. 6).
410 During low-RH pollution periods, NO_3^- and SO_4^{2-} showed a good correlation ($R^2 = 0.75$)
411 with a ratio of 2.1, indicating a similar photochemical production process. However,
412 during high-RH pollution periods, the ratio of NO_3^- to SO_4^{2-} decreased significantly to 0.40
413 with a lower correlation coefficient ($R^2 = 0.53$). The degraded temporal correlation
414 between nitrate and sulfate suggest different formation pathway of nitrate and sulfate
415 during high RH pollution periods. Aqueous-phase production of SO_4^{2-} become important
416 during those periods. Consistently, Fig. 7 shows that the sulfate oxidation ratio (SOR =
417 $[\text{SO}_4^{2-}]/([\text{SO}_4^{2-}] + [\text{SO}_2])$) increased exponentially with the increase of ALWC at RH >50%.

418 A strong correlation of the mass concentrations between OOA and NO_3^- was observed with
419 R^2 of 0.84 (Fig. 8a), possibly explained by the dominant contribution of photochemical
420 production for both OOA and NO_3^- . When considering the RH effect (color coded in Fig.
421 8a), it is found that the data are scattered around the regression line with uniform slope
422 when RH <70% but concentrated in a small area above the regression line when RH >70%,
423 suggesting that the OOA formation at RH >70% is probably promoted by aerosol water.
424 This is further supported by the linear increase of OOA with increasing SO_4^{2-} when RH
425 >70%, while the relationship between OOA and SO_4^{2-} was very scattered when RH <70%
426 (Fig. 8b).

427 4 Conclusion

428 We conducted online measurements of PM_1 in urban Beijing from 29 December 2014 to
429 27 February 2015. The average mass concentration of PM_1 was $73.8 \mu\text{g m}^{-3}$ and OA was the
430 most important component of PM_1 (52%), followed by nitrate (14%) and sulfate (10%).
431 Source apportionment of OA resolved five factors including HOA, COA, BBOA, CCOA, and
432 OOA, in which CCOA (32%) and OOA (32%) were the most important sources to OA. The
433 mass proportion of CCOA in OA showed a significant increase from clean period (25%) to
434 pollution periods (31-35%), highlighting the important role of coal burning in haze
435 formation in wintertime Beijing. The meteorological conditions (WD, WS, and RH) have a
436 significant impact on the chemical composition and evolution of PM_1 species. Nitrate had
437 a higher contribution during low-RH pollution days, implying the photochemical



438 oxidation process of nitrate formation. In contrast, the mass fraction of sulfate to PM_{10} was
439 much higher during high-RH pollution episodes compared to those during low-RH
440 pollution episodes. The data also showed the exponential increase of sulfate oxidation
441 ratio (SOR) with ALWC at high RH conditions. Both are consistent with the impacts of
442 aqueous-phase reactions on the formation of sulfate. As for the OOA formation, the strong
443 correlation between OOA and NO_3^- may be explained by the dominant role of
444 photochemical production on both species; aqueous-phase processes may add an
445 additional contribution to OOA formation under high RH condition, as indicated by the
446 linear increase of OOA with increasing SO_4^{2-} when $RH > 70\%$.

447 *Data availability.* Raw data used in this study are archived at the Institute of Earth
448 Environment, Chinese Academy of Sciences, and are available on request by contacting
449 the corresponding author.

450 *Supplement.* The Supplement related to this article is available online at

451 *Competing interests.* The authors declare that they have no conflict of interest.

452 *Author contributions.* RJH designed the study. Data analysis and interpretation were made
453 by YH, JD, and RJH. RJH, JD, and YH prepared the manuscript with contributions from all
454 authors.

455 *Acknowledgments.* This work was supported by the National Natural Science Foundation
456 of China (NSFC) under Grant No. 41925015, 91644219, 41877408 and 41675120, the
457 National Key Research and Development Program of China (No. 2017YFC0212701), the
458 Chinese Academy of Sciences (no. ZDBS-LY-DQC001), and the Cross Innovative Team fund
459 from the State Key Laboratory of Loess and Quaternary Geology (No. SKLLQGTD1801),
460 and the Irish Environmental Protection Agency and Science Foundation Ireland project of
461 OM-MaREI.



462 References

- 463 Alfarra, M. R., Prévôt, A. S. H., Szidat, S., Sandradewi, J., Weimer, S., Lanz, V. A., Schreiber, D.,
464 Mohr, M., and Baltensperger, U.: Identification of the mass spectral signature of organic
465 aerosols from wood burning emissions, *Environ. Sci. Technol.*, 41, 5770-5777, 2007.
- 466 An, Z., Huang, R.-J., Zhang, R., Tie, X., Li, G., Cao, J., Zhou, W., Shi, Z., Han, Y., Gu, Z., and Ji, Y.:
467 Severe haze in northern China: A synergy of anthropogenic emissions and
468 atmospheric processes, *Proc. Natl. Acad. Sci.*, 116(18), 8657-8666, 2019.
- 469 Canagaratna, M. R., Jayne, J. T., Ghertner, D. A., Herndon, S., Shi, Q., Jimenez, J. L., Silva, P. J.,
470 Williams, P., Lanni, T., Drewnick, F., Demerjian, K. L., Kolb, C. E., and Worsnop, D. R.:
471 Chase studies of particulate emissions from in-use New York City vehicles, *Aerosol Sci.*
472 *Tech.*, 38(6), 555-573, 2004.
- 473 Canagaratna, M. R., Jayne, J. T., Jimenez, J. L., Allan, J. D., Alfarra, M. R., Zhang, Q., Onasch, T.
474 B., Drewnick, F., Coe, H., Middlebrook, A., Delia, A., Williams, L. R., Trimborn, A. M.,
475 Northway, M. J., DeCarlo, P. F., Kolb, C. E., Davidovits, P., and Worsnop, D. R.: Chemical
476 and microphysical characterization of ambient aerosols with the Aerodyne aerosol
477 mass spectrometer, *Mass Spectro. Rev.*, 26(2), 185-222, [https://doi.org/10.100/mas.](https://doi.org/10.100/mas.20115)
478 20115, 2007.
- 479 Canonaco, F., Crippa, M., Slowik, J. G., Baltensperger, U., and Prévôt, A. S. H.: SoFi, an IGOR-
480 based interface for the efficient use of the generalized multilinear engine (ME-2) for
481 the source apportionment: ME-2 application to aerosol mass spectrometer data,
482 *Atmos. Meas. Tech.*, 6, 3649-3661, <https://doi.org/10.5194/amt-6-3649-2013>, 2013.
- 483 Canonaco, F., Slowik, J. G., Baltensperger, U., and Prévôt, A. S. H.: Seasonal differences in
484 oxygenated organic aerosol composition: implications for emissions sources and
485 factor analysis, *Atmos. Chem. Phys.*, 15, 6993-7002, [https://doi.org/10.5194/acp-15-](https://doi.org/10.5194/acp-15-6993-2015)
486 6993-2015, 2015.
- 487 Chow, J. C., Bachmann, J. D., Wierman, S. S.G., Mathai, C.V., Malm, W. C., White, W. H., Mueller,
488 P. K., Kumar, N., and Watson, J. G.: Visibility: Science and Regulation, *J. Air. Waste.*
489 *Manage.*, 52 (9), 973-999, 2002.
- 490 Crippa, M., Decarlo, P. F., Slowik, J. G., Mohr, C., Heringa, M. F., Chirico, R., Poulain, L., Freutel,
491 F., Sciare, J., Cozic, J., Di Marco, C. F., Elsasser, M., Nicolas, J., Marchand, Nicolas, Abidi, E.,
492 Wiedensohler, A., Drewnick, F., Schneider, J., Borrmann, S., Nemitz, E., Zimmermann, R.,
493 Jaffrezo, J.-L., Prévôt, A. S. H., and Baltensperger U.: Wintertime aerosol chemical
494 composition and source apportionment of the organic fraction in the metropolitan
495 area of Paris, *Atmos. Chem. Phys.*, 13, 961-981, [https://doi.org/10.5194/acp-13-961-](https://doi.org/10.5194/acp-13-961-2013)
496 2013, 2013.
- 497 DeCarlo, P. F., Kimmel, J. R., Trimborn, A., Northway, M. J., Jayne, J. T., Aiken, A. C., Gonin,
498 M., Fuhrer, K., Horvath, T., Docherty, K. S., Worsnop, D. R., and Jimenez, J. L.: Field-
499 deployable, high-resolution, time-of-flight aerosol mass spectrometer, *Anal. Chem.*,
500 78(24), 8281-8289, <https://doi.org/10.1021/ac061249n>, 2006.
- 501 DeCarlo, P. F., Ulbrich, I. M., Crouse, J., de Foy, B., Dunlea, E. J., Aiken, A. C., Knapp, D.,
502 Weinheimer, A. J., Campos, T., Wennberg, P. O., and Jimenez, J. L.: Investigation of the
503 sources and processing of organic aerosol over the Central Mexican Plateau from
504 aircraft measurements during MILAGRO, *Atmos. Chem. Phys.*, 10, 5257-5280,



- 505 <https://doi.org/10.5194/acp-10-5257-2010>, 2010.
- 506 Deng, X., Tie, X., Wu, D., Zhou, X. J., Bi, X. Y., Tan, H. B., Li, F., and Jaing, C. L.: Long-term trend
507 of visibility and its characterizations in the Pearl River Delta (PRD) region, China,
508 *Atmos. Environ.*, 42(7), 1424-1435, 2008.
- 509 Elser, M., Huang, R. J., Wolf, R., Slowik, J. G., Wang, Q., Canonaco, F., Li, G., Bozzetti, C.,
510 Daellenbach, K. R., Huang, Y., Zhang, R., Li, Z., Cao, J., Baltensperger, U., El-Haddad, I.,
511 and Prévôt, A. S. H.: New insights into PM_{2.5} chemical composition and sources in two
512 major cities in China during extreme haze events using aerosol mass spectrometry,
513 *Atmos. Chem. Phys.*, 16, 3207–3225, <https://doi.org/10.5194/acp-16-3207-2016>,
514 2016.
- 515 Forster, P., Ramaswamy, V., and Artaxo, P.: Changes in atmospheric constituents and in
516 radiative forcing, Cambridge University Press: Cambridge, United Kingdom, pp 129-
517 234, 2007.
- 518 Goldstein, A. H., and Galbally, I. E.: Known and unexplored organic constituents in the
519 earth's atmosphere, *Environ. Sci. Technol.*, 41 (5), 1514-1521, 2007.
- 520 Hennigan, C. J., Izumi, J., Sullivan, A. P., Weber, R. J., and Nenes, A.: A critical evaluation of
521 proxy methods used to estimate the acidity of atmospheric particles, *Atmos. Chem.*
522 *Phys.*, 15, 2775–2790, <https://doi.org/10.5194/acp-15-2775-2015>, 2015.
- 523 Hagler, G. S. W., Bergin, M. H., Salmon, L. G., Yu, J. Z., Wan, E. C. H., Zheng, M., Zeng, L. M.,
524 Kiang, C. S., Zhang, Y. H., Lau, A. K. H., and Schauer, J. J.: Source areas and chemical
525 composition of fine particulate matter in the Pearl River Delta region of China, *Atmos.*
526 *Environ.*, 40 (20), 3802-3815, 2006.
- 527 Han, S., Kondo, Y., Oshima, N., Takegawa, N., Miyazaki, Y., Hu, M., Lin, P., Deng, Z., Zhao, Y.,
528 Sugimoto, N., and Wu, Y.: Temporal variations of elemental carbon in Beijing, *J. Geophys.*
529 *Res. Atmos.*, 114, 2009.
- 530 He, L.-Y., Huang, X.-F., Xue, L., Hu, M., Lin, Y., Zheng, J., Zhang, R., and Zhang, Y.-H.: Submicron
531 aerosol analysis and organic source apportionment in an urban atmosphere in Pearl
532 River Delta of China using high-resolution aerosol mass spectrometry, *J. Geophys. Res.*
533 *Atmos.*, 116, D12, <https://doi.org/10.1029/2010JD014566>, 2011.
- 534 Hien, P. D., Bac, V. T., and Thinh, N. T. H.: PMF receptor modelling of fine and coarse PM₁₀,
535 in air masses governing monsoon conditions in Hanoi, northern Vietnam, *Atmos.*
536 *Environ.*, 38(2), 189-201, 2004.
- 537 Hu, W. W., Hu, M., Yuan, B., Jimenez, J. L., Tang, Q., Peng, J. F., Hu, W., Shao, M., Wang, M.,
538 Zheng, L. M., Wu, Y. S., Gong, Z. H., Huang, X. F., and He, L. Y.: Insights on organic aerosol
539 aging and the influence of coal combustion at a regional receptor site of central eastern
540 China, *Atmos. Chem. Phys.*, 13, 10095–10112, <https://doi.org/10.5194/acp-13-10095-2013>, 2013.
- 542 Hu, W., Hu, M., Hu, W., Jimenez, J. L., Yuan, B., Chen, W., Wang, M., Wu, Y., Chen, C., Wang, Z.,
543 Peng, J., Zeng, L., and Shao, M.: Chemical composition, sources, and aging process of
544 submicron aerosols in Beijing: Contrast between summer and winter, *J. Geophys. Res.*
545 *Atmos.*, 121(4), 1955–1977, <https://doi.org/10.1002/2015JD024020>, 2016.
- 546 Huang, R. J., Zhang, Y. L., Bozzetti, C., Ho, K. F., Cao, J. J., Han, Y. M., Daellenbach, K. R., Slowik,
547 J. G., Platt, S. M., Canonaco, F., Zotter, P., Wolf, R., Pieber, S. M., Bruns, E. A., Crippa, M.,
548 Ciarelli, G., Piazzalunga, A., Schwikowski, M., Abbaszade, G., Schnelle-Kreis, J.,



- 549 Zimmermann, R., An, Z., Szidat, S., Baltensperger, U., Haddad, I.E., and Prevot, A.S.H.:
550 High secondary aerosol contribution to particulate pollution during haze events in
551 China, *Nature*, 514, 218–222, 2014.
- 552 Huang, R.-J., Wang, Y., Cao, J., Lin, C., Duan, J., Chen, Q., Li, Y., Gu, Y., Yan, J., Xu, W., Fröhlich,
553 R., Canonaco, F., Bozzetti, C., Ovadnevaite, J., Ceburnis, D., Canagaratna, M. R., Jayne, J.,
554 Worsnop, D. R., El-Haddad, I., Prévôt, A. S. H., and O'Dowd, C. D.: Primary emissions
555 versus secondary formation of fine particulate matter in the most polluted city
556 (Shijiazhuang) in North China, *Atmos. Chem. Phys.*, 19, 2283–2298,
557 <https://doi.org/10.5194/acp-19-2283-2019>, 2019.
- 558 Huang, X.-F., Yu, J. Z., He, L.-Y., and Yuan, Z. B.: Water-soluble organic carbon and oxalate in
559 aerosols at a coastal urban site in China: Size distribution characteristics, sources, and
560 formation mechanisms, *J. Geophys. Res. Atmos.*, 111(D22), 2006.
- 561 Huang, X.-F., He, L.-Y., Hu, M., Canagaratna, M. R., Kroll, J. H., Ng, N. L., Zhang, Y.-H., Lin, Y.,
562 Xue, L., Sun, T.-L., Liu, X.-G., Shao, M., Jayne, J. T., and Worsnop, D. R.: Characterization
563 of submicron aerosols at a rural site in Pearl River Delta of China using an Aerodyne
564 High-Resolution Aerosol Mass Spectrometer, *Atmos. Chem. Phys.*, 11, 1865–1877,
565 <https://doi.org/10.5194/acp-11-1865-2011>, 2011.
- 566 Huang, X. F., He, L. Y., Xue, L., Sun, T. L., Zeng, L. W., Gong, Z. H., Hu, M., and Zhu, T.: Highly
567 time-resolved chemical characterization of atmospheric fine particles during 2010
568 Shanghai world expo, *Atmos. Chem. Phys.*, 12, 4897–4907, [https://doi.org/10.5194/
569 acp-12-4897-2012](https://doi.org/10.5194/acp-12-4897-2012), 2012.
- 570 Huang, X.-F., Xue L., Tian, X.-D., Shao, W. W., Sun, T. L., Gong, Z. H., Ju, W. W., Jiang, B., Hu, M.,
571 and He, L. Y.: Highly time-resolved carbonaceous aerosol characterization in Yangtze
572 River Delta of China: Composition, mixing state and secondary formation, *Atmos.
573 Environ.*, 64, 200–207, 2013.
- 574 Huffman, J. A., Docherty, K. S., Aiken, A. C., Cubison, M. J., Ulbrich, I. M., DeCarlo, P. F., Sueper,
575 D., Jayne, J. T., Worsnop, D. R., Ziemann, P. J., and Jimenez, J. L.: Chemically-resolved
576 aerosol volatility measurements from two megacity field studies, *Atmos. Chem. Phys.*,
577 9, 7161–7182, <https://doi.org/10.5194/acp-9-7161-2009>, 2009.
- 578 Jenkin, M. E.: Investigation of an oxidant-based methodology for AOT40 exposure
579 assessment in the UK, *Atmos. Environ.*, 94, 332–340, 2014.
- 580 Jimenez, J. L., Jayne, J. T., Shi, Q., Kolb, C. E., Worsnop, D. R., Yourshaw, I., Seinfeld, J. H., Flagan,
581 R. C., Zhang, X., Smith, K. A., Morris, J. W., and Davidovits, P.: Ambient aerosol sampling
582 with an Aerosol Mass Spectrometer, *J. Geophys. Res.-Atmos.*, 108, 8425,
583 doi:10.1029/2001JD001213, 2003.
- 584 Jimenez, J. L., Canagaratna, M. R., Donahue, N. M., Prevot, A. S. H., Zhang, Q., Kroll, J. H.,
585 DeCarlo, P. F., Allan, J. D., Coe, H., Ng, N. L., Aiken, A. C., Docherty, K. S., Ulbrich, I. M.,
586 Grieshop, A. P., Robinson, A. L., Duplissy, J., Smith, J. D., Wilson, K. R., Lanz, V. A., Hueglin,
587 C., Sun, Y. L., Tian, J., Laaksonen, A., Raatikainen, T., Rautiainen, J., Vaattovaara, P., Ehn,
588 M., Kulmala, M., Tomlinson, J. M., Collins, D. R., Cubison, M. J., Dunlea, J., Huffman, J. A.,
589 Onasch, T. B., Alfarra, M. R., Williams, P. I., Bower, K., Kondo, Y., Schneider, J., Drewnick,
590 F., Borrmann, S., Weimer, S., Demerjian, K., Salcedo, D., Cottrell, L., Griffin, R., Takami, A.,
591 Miyoshi, T., Hatakeyama, S., Shimojo, A., Sun, J. Y., Zhang, Y. M., Dzepina, K., Kimmel, J.



- 592 R., Sueper, D., Jayne, J. T., Herndon, S. C., Trimborn, A. M., Williams, L. R., Wood, E. C.,
593 Middlebrook, A. M., Kolb, C. E., Baltensperger, U., and Worsnop, D. R.: Evolution of
594 organic aerosols in the atmosphere, *Science*, 326, 1525–1529,
595 <https://doi.org/10.1126/science.1180353>, 2009.
- 596 Kadowaki, S.: On the nature of atmospheric oxidation processes of sulfur dioxide to sulfate
597 and of nitrogen dioxide to nitrate on the basis of diurnal variations of sulfate, nitrate,
598 and other pollutants in an urban area, *Environ. Sci. Technol.*, 20(12), 86–93, 1986.
- 599 Kanakidou, M., Seinfeld, J. H., Pandis, S. N., Barnes, I., Dentener, F. J., Facchini, M. C., Van
600 Dingenen, R., Ervens, B., Nenes, A., Nielsen, C. J., Swietlicki, E., Putaud, J. P., Balkanski,
601 Y., Fuzzi, S., Horth, J., Moortgat, G. K., Winterhalter, R., Myhre, C. E. L., Tsigaridis, K.,
602 Vignati, E., Stephanou, E. G., and Wilson, J.: Organic aerosol and global climate
603 modelling: a review, *Atmos. Chem. Phys.*, 5, 1053–1123, <https://doi.org/10.5194/acp-5-1053-2005>, 2005.
- 605 Khoder, M. I.: Atmospheric conversion of sulfur dioxide to particulate sulfate and nitrogen
606 dioxide to particulate nitrate and gaseous nitric acid in an urban area, *Chemosphere*,
607 49(6), 675–84, 2002.
- 608 Lanz, V. A., Alfarra, M. R., Baltensperger, U., Buchmann, B., Hueglin, C., and Prévôt, A. S. H.:
609 Source apportionment of submicron organic aerosols at an urban site by factor
610 analytical modelling of aerosol mass spectra, *Atmos. Chem. Phys.*, 7, 1503–1522,
611 <https://doi.org/10.5194/acp-7-1503-2007>, 2007.
- 612 Lanz, V. A., Prévôt, A. S. H., Alfarra, M. R., Weimer, S., Mohr, C., DeCarlo, P. F., Gianini, M. F. D.,
613 Hueglin, C., Schneider, J., Favez, O., D'Anna, B., George, C., and Baltensperger, U.:
614 Characterization of aerosol chemical composition with aerosol mass spectrometry in
615 Central Europe: an overview, *Atmos. Chem. Phys.*, 10, 10453–10471,
616 <https://doi.org/10.5194/acp-10-10453-2010>, 2010.
- 617 Lee, B. P., Li, Y. J., Yu, J. Z., Louie, P. K. K., and Chan, C. K.: Characteristics of submicron
618 particulate matter at the urban roadside in downtown Hong Kong Overview of 4
619 months of continuous high-resolution aerosol mass spectrometer measurements, *J.*
620 *Geophys. Res.-Atmos.*, 120 (14), 7040–7058, 2015.
- 621 Li, Y. J., Lee, B. P., Su, L., Fung, J. C. H., and Chan, C. K.: Seasonal characteristics of fine
622 particulate matter (PM) based on high resolution time-of-flight aerosol mass
623 spectrometric (HR-ToF AMS) measurements at the HKUST Supersite in Hong Kong,
624 *Atmos. Chem. Phys.*, 15, 37–53, <https://doi.org/10.5194/acp-15-37-2015>, 2015.
- 625 Lu, K., Fuchs, H., Hofzumahaus, A., Tan, Z., Wang, H., Zhang, L., Schmitt, S. H., Rohrer, F.,
626 Bohn, B., Broch, S., Dong, H., Gkatzelis, G. I., Hohaus, T., Holland, F., Li, X., Liu, Y., Ma, X.,
627 Novelli, A., Schlag, P., Shao, M., Wu, Y., Wu, Z., Zeng, L., Hu, M., Kiendler-Scharr, A.,
628 Wahner, A., and Zhang, Y.: Fast Photochemistry in Wintertime Haze: Consequences for
629 Pollution Mitigation Strategies, *Environ. Sci. Technol.*, 53(18), 10676–10684, 2019.
- 630 Massoli, P., Fortner, E. C., Canagaratna, M. R., Williams, L. R., Zhang, Q., Sun, Y. L., Schwab, J.
631 J., Trimborn, A., Onasch, T. B., Demerjian, K. L., Kolb, C. E., Worsnop, D. R., and Jayne, J.
632 T.: Pollution Gradients and Chemical Characterization of Particulate Matter from
633 Vehicular Traffic Near Major Roadways: Results from the 2009 Queens College Air
634 Quality Study in NYC, *Aerosol Sci. Tech.*, 46, 1201–1218,
635 [doi:10.1080/02786826.2012.701784](https://doi.org/10.1080/02786826.2012.701784), 2012. Matson, P., Lohse, K. A., and Hall, S. J.: The



- 636 globalization of nitrogen deposition: Consequences for terrestrial ecosystems, *Ambio*,
637 31 (2), 113-119,2002.
- 638 Murphy, J. G., Day, D. A., and Cleary, P. A.: The weekend effect within and downwind of
639 Sacramento – Part 1: Observations of ozone, nitrogen oxides, and VOC reactivity,
640 *Atmos. Chem. Phys.*, 7(20), 5327-5339, 2007.
- 641 Nilsson, P. T., Eriksson, A. C., Ludvigsson, L., Messing, M. E., Nordin, E. Z., Gudmundsson, A.,
642 Meuller, B. O., Deppert, K., Fortner, E. C., Onasch, T. B., and Pagels, J. H.: In-situ
643 characterization of metal nanoparticles and their organic coatings using laser-
644 vaporization aerosol mass spectrometry, *Nano Research*, 8 (12), 3780-3795, 2015.
- 645 Ng, N. L., Herndon, S. C., Trimborn, A., Canagaratna, M. R., Croteau, P. L., Onasch, T. B., Sueoer,
646 D., Worsnop, D. R., Zhang, Q., Sun, Y. L., and Jayne, J. T.: An Aerosol Chemical Speciation
647 Monitor (ACSM) for routine monitoring of the composition and mass concentrations
648 of ambient aerosol, *Aerosol Sci. Technol.*, 45 (7), 770-784,
649 <https://doi.org/10.1080/02786826.2011.560211>, 2011a.
- 650 Ng, N. L., Canagaratna, M. R., Jimenez, J. L., Zhang, Q., Ulbrich, M., and Worsnop, D. R.: Real-
651 time methods for estimating organic component mass concentrations from aerosol
652 mass spectrometer data, *Environ. Sci. Technol.*, 45, 910-916, [https://doi.org/10.1021](https://doi.org/10.1021/es102951k)
653 /[es102951k](https://doi.org/10.1021/es102951k), 2011b.
- 654 Paatero, P., and Tapper, U.: Positive matrix factorization: A non-negative factor model with
655 optimal utilization of error estimates of data values, *Environmetrics*, 5 (2), 111-126,
656 1994.
- 657 Peng, R. D., Dominici, F., Pastor-Barriuso, R., Zeger, S. L., and Samet, J. M.: Seasonal analyses
658 of air pollution and mortality in 100 US cities, *Am. J. Epidemiol.*, 161 (6), 585-594,
659 2005.Pope, C. A., Burnett, R. T., Thun, M. J., Calle, E. E., Krewski, D., Ito, K., and Thurston,
660 G. D.: Lung cancer, cardiopulmonary mortality, and long-term exposure to fine
661 particulate air pollution, *J. Am. Med. Assoc.*, 287, 1132-1141, 2002.
- 662 Pudasainee, D., Sapkota, B., Bhatnagar, A., Kim, S. H., and Seo, Y. C.: Influence of weekdays,
663 weekends and bandhas on surface ozone in Kathmandu valley, *Atmos. Res.*, 95(2-3),
664 150-156, 2010.
- 665 Schauer, J. J., Rogge, W. F., Hildemann, L. M., Mazurek, M. A., Cass, G. R., and Simoneit, B. R.:
666 Source apportionment of airborne particulate matter using organic compounds as
667 tracers, *Atmos. Environ.*, 30 (22), 3837-3855, 1996.
- 668 Schneider, J., Weimer, S., Drewnick, F., Borrmann, S., Helas, G., Gwaze, P., Schmid, O.,
669 Andreae, M.O. and Kirchner, U.: Mass spectrometric analysis and aerodynamic
670 properties of various types of combustion-related aerosol particles, *Int. J. Mass*
671 *Spectrom.*, 258(1-3), 37-49, 2006.
- 672 Seinfeld, J. H., Pandis, S. N., and Noone, K.: Atmospheric chemistry and physics: from air
673 pollution to climate change, *Physics Today*, 51, 88, 1998.
- 674 Shao, J., Chen, Q., Wang, Y., Lu, X., He, P., Sun, Y., Shah, V., Martin, R. V., Philip, S., Song, S.,
675 Zhao, Y., Xie, Z., Zhang, L., and Alexander, B.: Heterogeneous sulfate aerosol formation
676 mechanisms during wintertime Chinese haze events: air quality model assessment
677 using observations of sulfate oxygen isotopes in Beijing, *Atmos. Chem. Phys.*, 19, 6107-
678 6123, <https://doi.org/10.5194/acp-19-6107-2019>, 2019.
- 679 Song, S., Nenes, A., Gao, M., Zhang, Y., Liu, P., Shao, J., Ye, D., Xu, W., Lei, L., Sun, Y., Liu, B.,



- 680 Wang, S., and McElroy, M.: Thermodynamic modeling suggests declines in water
681 uptake and acidity of inorganic aerosols in Beijing winter haze events during
682 2014/2015–2018/2019, *Environ. Sci. & Tech. Let.*, 6(12), 752–760, 2019.
- 683 Sun, C., Lee, B. P., Huang, D., Jie Li, Y., Schurman, M. I., Louie, P. K. K., Luk, C., and Chan, C. K.:
684 Continuous measurements at the urban roadside in an Asian megacity by Aerosol
685 Chemical Speciation Monitor (ACSM): particulate matter characteristics during fall
686 and winter seasons in Hong Kong, *Atmos. Chem. Phys.*, 16, 1713–1728,
687 <https://doi.org/10.5194/acp-16-1713-2016>, 2016.
- 688 Sun, Y. L., Zhang, Q., Schwab, J. J., Demerjian, K. L., Chen, W. N., Bae, M. S., Hung, H. M.,
689 Hogrefe, O., Frank, B., Rattigan, O. V., and Lin, Y. C.: Characterization of the sources and
690 processes of organic and inorganic aerosols in New York city with a high-resolution
691 time-of-flight aerosol mass spectrometer, *Atmos. Chem. Phys.*, 11, 1581–1602,
692 [doi:10.5194/acp-11-1581-2011](https://doi.org/10.5194/acp-11-1581-2011), 2011.
- 693 Sun, Y. L., Wang, Z., Dong, H., Yang, T., Li, J., Pan, X., Chen, P., and Jayne, J. T.: Characterization
694 of summer organic and inorganic aerosols in Beijing, China with an Aerosol Chemical
695 Speciation Monitor, *Atmos. Environ.*, 51, 250–259,
696 [doi:10.1016/j.atmosenv.2012.01.013](https://doi.org/10.1016/j.atmosenv.2012.01.013), 2012.
- 697 Sun, Y. L., Wang, Z. F., Fu, P. Q., Yang, T., Jiang, Q., Dong, H. B., Li, J., and Jia, J. J.: Aerosol
698 composition, sources and processes during wintertime in Beijing, China, *Atmos. Chem.
699 Phys.*, 13, 4577–4592, <https://doi.org/10.5194/acp-13-4577-2013>, 2013.
- 700 Sun, Y. L., Wang, Z. F., Fu, P. Q., Jiang, Q., Yang, T., Li, J., and Ge, X. L.: The impact of relative
701 humidity on aerosol composition and evolution processes during wintertime in
702 Beijing, China, *Atmos. Environ.*, 77, 927–934, 2013.
- 703 Sun, Y., Jiang, Q., Wang, Z., Fu, P., Li, J., Yang, T., and Yin, Y.: Investigation of the sources and
704 evolution processes of severe haze pollution in Beijing in January 2013, *J. Geophys. Res.
705 Atmos.*, 119, 4380–4398, <https://doi.org/10.1002/2014JD021641>, 2014.
- 706 Sun, Y. L., Wang, Z. F., Du, W., Zhang, Q., Wang, Q. Q., Fu, P. Q., Pan, X., Li, J., Jayne, J., and
707 Worsnop, D. R.: Long-term real-time measurements of aerosol particle composition in
708 Beijing, China: seasonal variations, meteorological effects, and source analysis, *Atmos.
709 Chem. Phys.*, 15, 10149–10165, <https://doi.org/10.5194/acp-15-10149-2015>, 2015.
- 710 Sun, Y., Du, W., Fu, P., Wang, Q., Li, J., Ge, X., Zhang, Q., Zhu, C., Ren, L., Xu, W., Zhao, J., Han, T.,
711 Worsnop, D. R., and Wang, Z.: Primary and secondary aerosols in Beijing in winter:
712 sources, variations and processes, *Atmos. Chem. Phys.*, 16, 8309–8329,
713 <https://doi.org/10.5194/acp-16-8309-2016>, 2016.
- 714 Ulbrich, I. M., Canagaratna, M. R., Zhang, Q., Worsnop, D. R., and Jimenez, J. L.:
715 Interpretation of organic components from Positive Matrix Factorization of aerosol
716 mass spectrometric data, *Atmos. Chem. Phys.*, 9, 2891–2918, <https://doi.org/10.5194/acp-9-2891-2009>, 2009.
- 718 Vecchi, R., Marazzan, G., Valli, G., Ceriani, M., and Antoniazzi, C.: The role of atmospheric
719 dispersion in the seasonal variation of PM₁ and PM_{2.5} concentration and composition
720 in the urban area of Milan (Italy), *Atmos. Environ.*, 38 (27), 4437–4446, 2004.
- 721 Wang, Y. C., Huang, R. J., Ni, H. Y., Chen, Y., Wang, Q. Y., Li, G. H., Tie, X. X., Shen, Z. X., Huang,
722 Y., Liu, S. X., Dong, W. M., Xue, P., Fröhlich, R., Canonaco, F., Elser, M., Daellenbach, K.R.,
723 Bozzetti, C., Haddad, E.I., and Cao, J. J.: Chemical composition, sources and secondary



- 724 processes of aerosols in Baoji city of northwest China, *Atmos. Environ.*, 158, 128–137,
725 <https://doi.org/10.1016/j.atmosenv.2017.03.026>, 2017.
- 726 Wu, Y. Z., Ge, X. L., Wang, J. F., Shen, Y. F., Ye, Z. L., Ge, S., Wu, Y., Yu, H., and Chen, M. D.:
727 Responses of secondary aerosols to relative humidity and photochemical activities in
728 an industrialized environment during late winter, *Atmos. Environ.*, 193, 66–78, 2018.
- 729 Xu, W. Q., Han, T. T., Du, W., Wang, Q. Q., Chen, C., Zhao, J., Zhang, Y. J., Li, J., Fu, P. Q., Wang, Z.
730 F., Worsnop, D. R., and Sun, Y. L.: Effects of Aqueous-Phase and Photochemical
731 Processing on Secondary Organic Aerosol Formation and Evolution in Beijing, China,
732 *Environ. Sci. Technol.*, 51(2), 762–770, <https://doi.org/10.1021/acs.est.6b04498>,
733 2017.
- 734 Xu, W. Q., Sun, Y. L., Wang, Q. Q., Zhao, J., Wang, J. F., Ge, X. L., Xie, C. H., Zhou, W., Du, W., Li,
735 J., Fu, P. Q., Wang, Z. F., Worsnop, D. R., and Coe, H.: Changes in aerosol chemistry from
736 2014 to 2016 in winter in Beijing: insights from high resolution aerosol mass
737 spectrometry, *J. Geophys. Res. Atmos.*, 124(2), 1132–1147, 2018.
- 738 Zhang, Q., Alfarra, M. R., Worsnop, D. R., Allan, J. D., Coe, H., Canagaratna, M. R., and Jimenez,
739 J. L.: Deconvolution and quantification of hydrocarbon-like and oxygenated organic
740 aerosols based on aerosol mass spectrometry, *Environ. Sci. Technol.*, 39 (13), 4938–
741 4952, 2005.
- 742 Zhang, Q., Jimenez, J. L., Canagaratna, M. R., Allan, J. D., Coe, H., Ulbrich, I., and Dzepina, K.:
743 Ubiquity and dominance of oxygenated species in organic aerosols in
744 anthropogenically-influenced Northern Hemisphere midlatitudes, *Geophys. Res. Lett.*,
745 34 (13), 2007.
- 746 Zhang, Q., Meng, J., Quan, J., Gao, Y., Zhao, D., Chen, P., and He, H.: Impact of aerosol
747 composition on cloud condensation nuclei activity, *Atmos. Chem. Phys.*, 12, 3783–
748 3790, <https://doi.org/10.5194/acp-12-3783-2012>, 2012.
- 749 Zhang, Y., Schauer, J. J., Zhang, Y., Zeng, L., Wei, Y., Liu, Y., and Shao, M.: Characteristics of
750 particulate carbon emissions from real-world Chinese coal combustion, *Environ. Sci.*
751 *Technol.*, 42 (14), 5068–5073, 2008.
- 752 Zhang, Y., Tang, L., Yu, H., Wang, Z., Sun, Y., Qin, W., and Ge, S.: Chemical composition,
753 sources and evolution processes of aerosol at an urban site in Yangtze River Delta,
754 China during wintertime, *Atmos. Environ.*, 123, 339–349, 2015a.
- 755 Zhang, Y. J., Tang, L. L., Wang, Z., Yu, H. X., Sun, Y. L., Liu, D., and Zhou, H. C.: Insights into
756 characteristics, sources, and evolution of submicron aerosols during harvest seasons
757 in the Yangtze River delta region, China. *Atmos. Chem. and Phys.*, 15(3), 1331–1349.
- 758 Zhang, Y. M., Zhang, X. Y., Sun, J. Y., Lin, W. L., Gong, S. L., Shen, X. J., and Yang, S.:
759 Characterization of new particle and secondary aerosol formation during summertime
760 in Beijing, China, *Tellus B.*, 63(3), 382–394, 2011.
- 761 Zhang, Y. J., Tang, L. L., Sun, Y. L., Favez, O., Canonaco, F., Albinet, A., Couvidat, F., Liu, D. T.,
762 Jayne, J. T., Wang, Z., Croteau, P. L., Canagaratna, M. R., Zhou, H. C., Prevot, A. S. H., and
763 Worsnop, D.R.: Limited formation of isoprene epoxydiols-derived secondary organic
764 aerosol under NO_x - rich environments in Eastern China, *Geophys. Res. Lett.*, 44(4),
765 2035 – 2043, <https://doi.org/10.1002/2016GL072368>, 2017.
- 766 Zheng, B., Zhang, Q., Zhang, Y., He, K. B., Wang, K., Zheng, G. J., Duan, F. K., Ma, Y. L., and
767 Kimoto, T.: Heterogeneous chemistry: a mechanism missing in current models to



768 explain secondary inorganic aerosol formation during the January 2013 haze episode
769 in North China, Atmos. Chem. Phys., 15, 2031–2049, <https://doi.org/10.5194/acp-15->
770 2031-2015, 2015.

771

772



773 **Table1** Summary of the PM₁ composition, OA sources and meteorological conditions
 774 during different pollution periods.

Species	Clean	High-RH pollution	Low-RH pollution
PM ₁ (μg m ⁻³)	19.5	123.2	125.4
Org (μg m ⁻³)	10.9 (56%)	56.7 (46%)	67.7 (54%)
SO ₄ ²⁻ (μg m ⁻³)	2.0 (10%)	20.9 (17%)	8.8 (7%)
NO ₃ ⁻ (μg m ⁻³)	2.2 (11%)	17.2 (14%)	18.8 (15%)
NH ₄ ⁺ (μg m ⁻³)	1.8 (9%)	12.3 (10%)	11.3 (9%)
Cl ⁻ (μg m ⁻³)	1 (5%)	7.4 (6%)	8.8 (7%)
BC (μg m ⁻³)	1.7 (9%)	8.6 (7%)	10.0 (8%)
HOA (μg m ⁻³)	0.8 (8%)	9.1 (16%)	8.8 (13%)
COA (μg m ⁻³)	2 (20%)	6.8(12%)	8.8 (13%)
BBOA (μg m ⁻³)	1 (10%)	3.4 (6%)	8.1 (12%)
CCOA (μg m ⁻³)	2.8 (25%)	17.6 (31%)	23.7 (35%)
OOA (μg m ⁻³)	4.1 (37%)	19.8 (35%)	18.3 (27%)
O _x (ppb)	39.2	47.8	59.8
NO ₂ (ppb)	16.7	64.3	103.0
RH (%)	25	60	31
WS (m s ⁻¹)	2.5	1	0.9
Vis (Km)	15.7	6.5	6.7

775

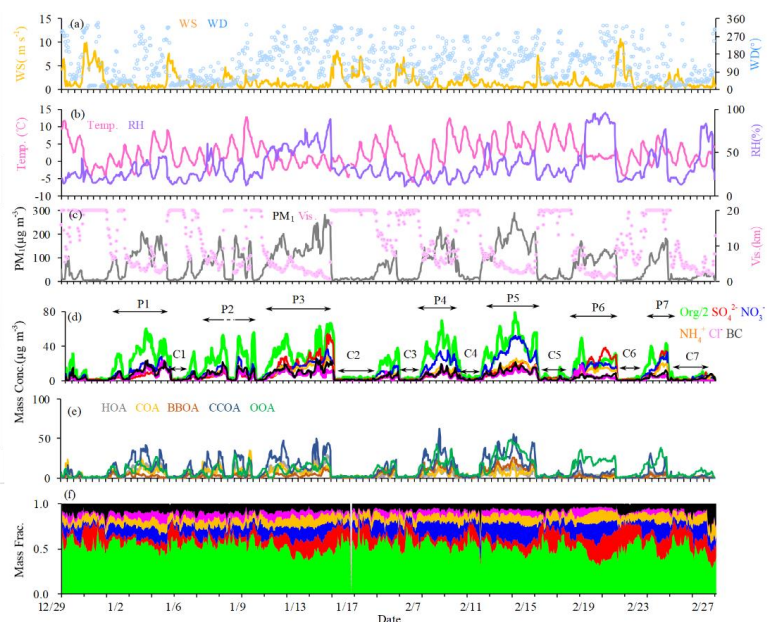
776

777



778

779



780

781 **Figure 1.** Time series of (a) wind speed (WS) and wind direction (WD), (b) Temperature
782 (Temp) and relative humidity (RH), (c) visibility and PM₁, (d) NR-PM₁ species (i.e., OA,
783 SO₄²⁻, NO₃⁻, NH₄⁺, Cl⁻ and BC; note that OA is halved clarity), (e) OA factors (i.e., HOA, COA,
784 BBOA, CCOA and OOA), and (f) relative contribution of PM₁ species.

785

786

787

788

789

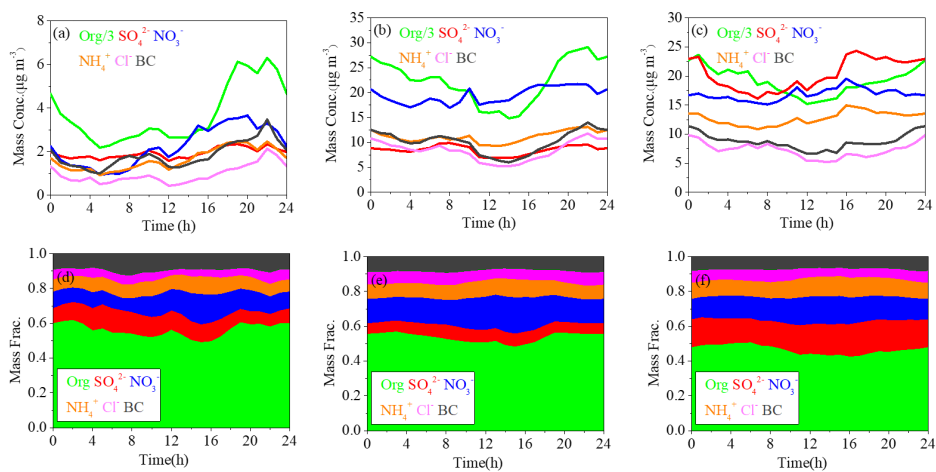
790

791

792



793



794

795 **Figure 2.** The diurnal variations of mass concentrations and relative contributions of PM₁
796 components during clean days (a, d), low-RH pollution days (b, e) and high-RH pollution
797 days (c, f).

798

799

800

801

802

803

804

805

806

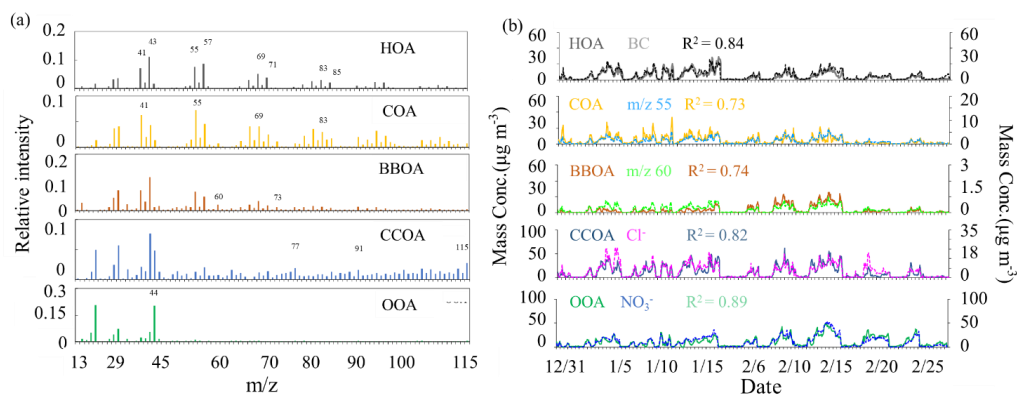
807

808



809

810



811

812 **Figure 3.** The mass spectra(a) and time series(b) of OA factors (HOA, COA, BBOA, CCOA,
813 and OOA).

814

815

816

817

818

819

820

821

822

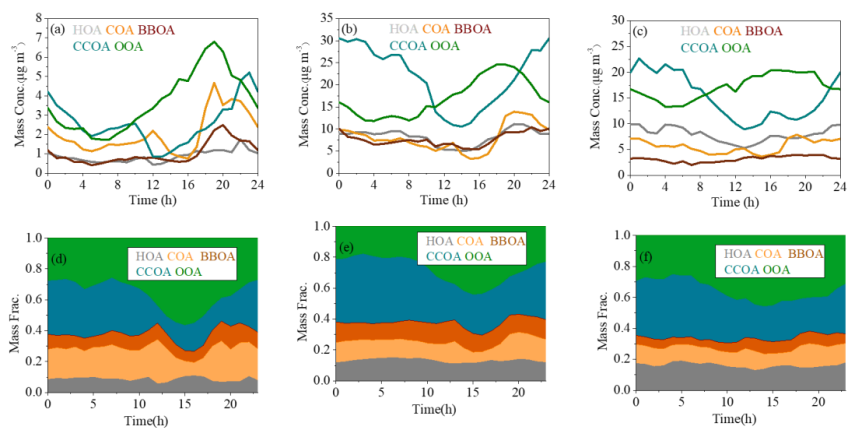
823

824

825



826

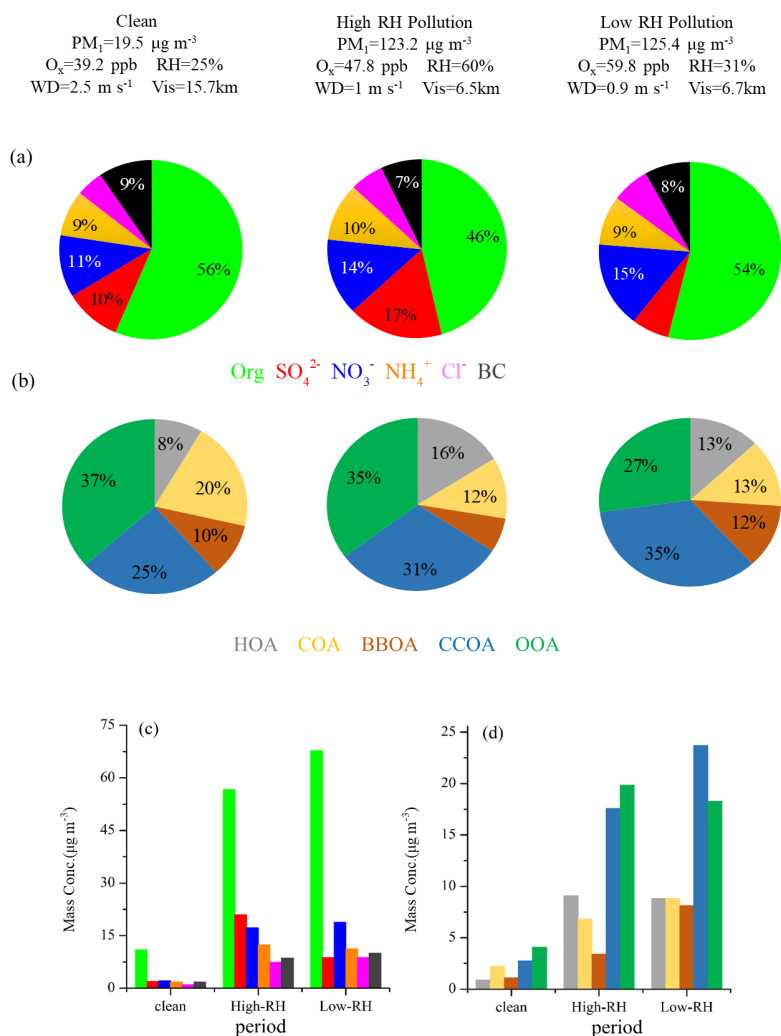


827

828 **Figure 4.** The diurnal variations of mass concentrations and relative contributions of OA
829 factors during clean days (a, d), low-RH pollution days (b, e) and high-RH pollution
830 days (c, f).

831

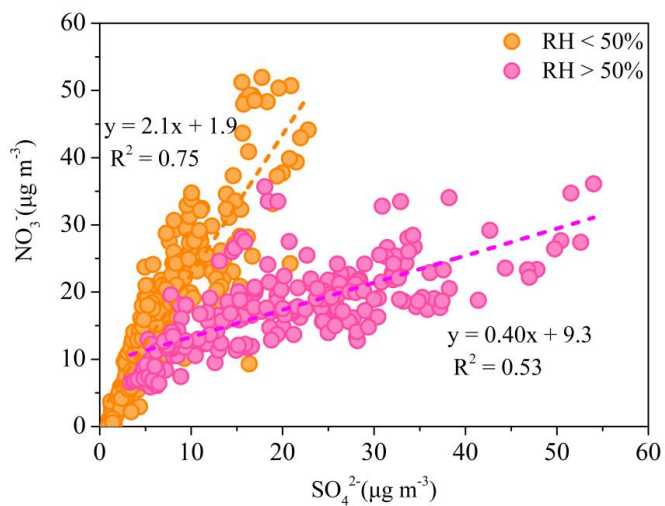
832



833

834 **Figure 5.** PM₁₀ chemical composition (a) and OA source composition (b) pie chart as well
 835 as the mass concentrations of PM₁₀ species(c) and OA sources(d) during clean, High-RH
 836 pollution and Low-RH pollution periods.

837



838

839 **Figure 6.** The relationship between SO_4^{2-} and NO_3^- during low-RH ($\text{RH} < 50\%$) and high-
840 RH ($\text{RH} > 50\%$) pollution episodes.

841

842

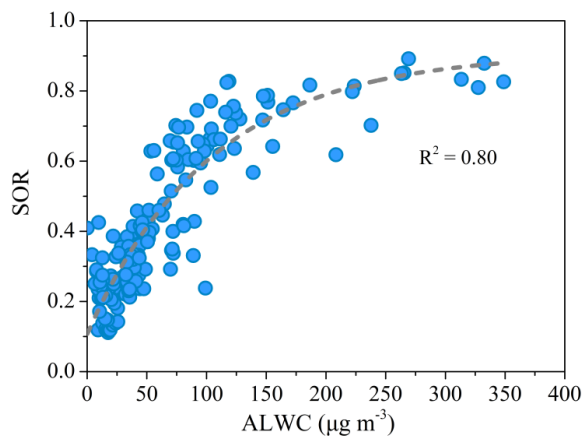
843

844

845

846

847



848

849 **Figure 7.** The relationship between the sulfate oxidation ratio ($SOR = [SO_4^{2-}]/([SO_4^{2-}] +$
850 $[SO_2])$) and ALWC at high RH condition ($RH > 50\%$).

851

852

853

854

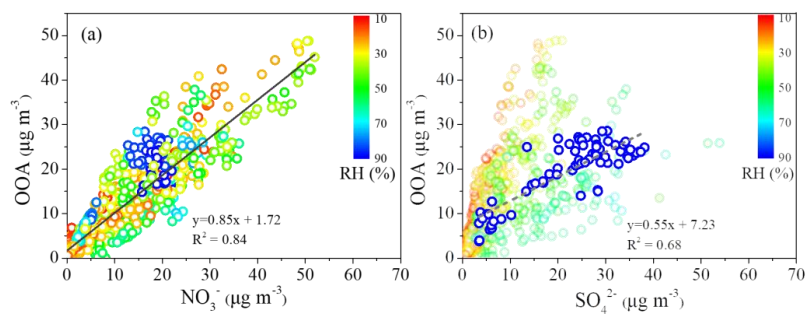
855

856

857

858

859



860

861 **Figure 8.** Scatter plot between the mass concentration of OOA and NO_3^- (colored by RH)
862 (a), and scatter plot between the mass concentration of OOA and SO_4^{2-} (colored by RH)
863 (b).

864